1.1 Resonant absorption and fluorescence

Before delving into the details of the subject, it is worthwhile considering the historical perspective of what has come to be considered as a discovery of prime importance.

Atomic resonant fluorescence was predicted and discovered just after the turn of the century, and within a few years the underlying theory had been developed. From a simplified viewpoint, an atom in an excited electronic state can decay to its ground state by the emission of a photon to carry off the excess energy. This photon can then be absorbed by a second atom of the same kind by electronic excitation. Subsequent de-excitation re-emits the photon, but not necessarily in the initial direction so that scattering or resonant fluorescence occurs. Thus if the monochromatic yellow light from a sodium lamp is collimated and passed through a glass vessel containing sodium vapour, one would expect to see a yellow glow as the incident beam is scattered by resonant fluorescence.

A close parallel can be drawn between atomic and nuclear resonant absorption. The primary decay of the majority of radioactive nuclides produces a daughter nucleus which is in a highly excited state. The latter then de-excites by emitting a series of γ-ray photons until by one or more routes, depending on the complexity of the γ-cascade, it reaches a stable ground state. This is clearly analogous to electronic de-excitation, the main difference being in the much higher energies involved in nuclear transitions. It was recognized in the 1920's that it should be possible to use the γ-ray emitted during a transition to a nuclear ground-state to excite a second stable nucleus of the same isotope, thus giving rise to nuclear resonant absorption and fluorescence.

The first experiments to detect these resonant processes by Kuhn in 1929 [2] were a failure, although it was already recognized that the nuclear recoil and Doppler broadening effects (to be discussed shortly) were probably responsible. Continuing attempts to observe nuclear resonant absorption [3] were inspired by the realization that the emitted γ-rays should be an unusually good source of monochromatic radiation. This can easily be shown from the Heisenberg uncertainty principle. The ground state of the nucleus has an infinite lifetime and therefore there is no uncertainty in its energy. The uncertainty in the lifetime of

the excited state is given by its mean life τ, and the uncertainty in its energy is given by the width of the statistical energy distribution at half-height Γ. They are related by

$$\Gamma\tau \geqslant \hbar \tag{1.1}$$

where h ($=2\pi\hbar$) is Planck's constant. τ is related to the more familiar half-life of the state by $\tau = \ln 2 \times t_{1/2}$. If Γ is given in electron-volts (1 eV = 1.60219×10^{-19} J and is equivalent to 96.49 kJ mol^{-1}) and $t_{1/2}$ in seconds, then

$$\Gamma = 4.562 \times 10^{-16}/t_{1/2} \tag{1.2}$$

For a typical nuclear excited-state half-life of $t_{1/2} = 10^{-7}$ s, $\Gamma = 4.562 \times 10^{-9}$ eV. If the energy of the excited state is 45.62 keV, the emitted γ-ray will have an intrinsic resolution of 1 part in 10^{13}. It should be borne in mind that the maximum resolution obtained in atomic line spectra is only about 1 in 10^8.

The nucleus is normally considered to be independent of the chemical state of the atom because of the great disparity between nuclear and chemical energies. However, the γ-ray energy is so sharply defined that Γ is smaller in magnitude than some of the interactions of the nucleus with its chemical environment. The typical magnitudes of some of the energies involved are indicated in Table 1.1.

Unfortunately there are several mechanisms which can degrade the energy of the emitted γ-ray, particularly the effects of the nuclear recoil and thermal energy [3]. Consider an isolated nucleus of mass M with an excited state level at an energy E and moving with a velocity V along the direction in which the γ-ray is to be emitted (the components of motion perpendicular to this direction remain unaffected by the decay and may be ignored). The energy above the ground state *at rest* is $(E + \frac{1}{2}MV^2)$. When a γ-ray of energy E_γ is emitted, the nucleus recoils and has a new velocity $V + v$ (which is a vector sum in that V and v may be opposed) and a total energy of $\frac{1}{2}M(V+v)^2$. By conservation of energy

$$E + \tfrac{1}{2}MV^2 = E_\gamma + \tfrac{1}{2}M(V+v)^2 \tag{1.3}$$

1.1 Resonant absorption and fluorescence

Before delving into the details of the subject, it is worthwhile considering the historical perspective of what has come to be considered as a discovery of prime importance.

Atomic resonant fluorescence was predicted and discovered just after the turn of the century, and within a few years the underlying theory had been developed. From a simplified viewpoint, an atom in an excited electronic state can decay to its ground state by the emission of a photon to carry off the excess energy. This photon can then be absorbed by a second atom of the same kind by electronic excitation. Subsequent de-excitation re-emits the photon, but not necessarily in the initial direction so that scattering or resonant fluorescence occurs. Thus if the monochromatic yellow light from a sodium lamp is collimated and passed through a glass vessel containing sodium vapour, one would expect to see a yellow glow as the incident beam is scattered by resonant fluorescence.

A close parallel can be drawn between atomic and nuclear resonant absorption. The primary decay of the majority of radioactive nuclides produces a daughter nucleus which is in a highly excited state. The latter then de-excites by emitting a series of γ-ray photons until by one or more routes, depending on the complexity of the γ-cascade, it reaches a stable ground state. This is clearly analogous to electronic de-excitation, the main difference being in the much higher energies involved in nuclear transitions. It was recognized in the 1920's that it should be possible to use the γ-ray emitted during a transition to a nuclear ground-state to excite a second stable nucleus of the same isotope, thus giving rise to nuclear resonant absorption and fluorescence.

The first experiments to detect these resonant processes by Kuhn in 1929 [2] were a failure, although it was already recognized that the nuclear recoil and Doppler broadening effects (to be discussed shortly) were probably responsible. Continuing attempts to observe nuclear resonant absorption [3] were inspired by the realization that the emitted γ-rays should be an unusually good source of monochromatic radiation. This can easily be shown from the Heisenberg uncertainty principle. The ground state of the nucleus has an infinite lifetime and therefore there is no uncertainty in its energy. The uncertainty in the lifetime of

the excited state is given by its mean life τ, and the uncertainty in its energy is given by the width of the statistical energy distribution at half-height Γ. They are related by

$$\Gamma\tau \geqslant \hbar \tag{1.1}$$

where h ($=2\pi\hbar$) is Planck's constant. τ is related to the more familiar half-life of the state by $\tau = \ln 2 \times t_{1/2}$. If Γ is given in electron-volts (1 eV = 1.60219×10^{-19} J and is equivalent to 96.49 kJ mol^{-1}) and $t_{1/2}$ in seconds, then

$$\Gamma = 4.562 \times 10^{-16}/t_{1/2} \tag{1.2}$$

For a typical nuclear excited-state half-life of $t_{1/2} = 10^{-7}$ s, $\Gamma = 4.562 \times 10^{-9}$ eV. If the energy of the excited state is 45.62 keV, the emitted γ-ray will have an intrinsic resolution of 1 part in 10^{13}. It should be borne in mind that the maximum resolution obtained in atomic line spectra is only about 1 in 10^8.

The nucleus is normally considered to be independent of the chemical state of the atom because of the great disparity between nuclear and chemical energies. However, the γ-ray energy is so sharply defined that Γ is smaller in magnitude than some of the interactions of the nucleus with its chemical environment. The typical magnitudes of some of the energies involved are indicated in Table 1.1.

Unfortunately there are several mechanisms which can degrade the energy of the emitted γ-ray, particularly the effects of the nuclear recoil and thermal energy [3]. Consider an isolated nucleus of mass M with an excited state level at an energy E and moving with a velocity V along the direction in which the γ-ray is to be emitted (the components of motion perpendicular to this direction remain unaffected by the decay and may be ignored). The energy above the ground state *at rest* is $(E + \frac{1}{2}MV^2)$. When a γ-ray of energy E_γ is emitted, the nucleus recoils and has a new velocity $V + v$ (which is a vector sum in that V and v may be opposed) and a total energy of $\frac{1}{2}M(V + v)^2$. By conservation of energy

$$E + \tfrac{1}{2}MV^2 = E_\gamma + \tfrac{1}{2}M(V + v)^2 \tag{1.3}$$

Table 1.1 Typical energies of nuclear and chemical interactions

Mössbauer γ-ray energies (E_γ)	10^6–10^7	kJ mol^{-1}
Chemical bonds and lattice energies	10^2–10^3	kJ mol^{-1}
Electronic transitions	50–500	kJ mol^{-1}
Molecular vibrations	5–50	kJ mol^{-1}
Lattice vibrations	0.5–5	kJ mol^{-1}
Nuclear recoil and Doppler energies (E_R, E_D)	10^{-2}–1	kJ mol^{-1}
Nuclear quadrupole coupling constants	$<10^{-3}$	kJ mol^{-1}
Nuclear Zeeman splittings	$<10^{-3}$	kJ mol^{-1}
Heisenberg linewidths (Γ)	10^{-7}–10^{-4}	kJ mol^{-1}

1 eV = 1.60219 x 10^{-19} J and is equivalent to 96.49 kJ mol^{-1}

so that the actual energy of the photon emitted is given by

$$E_\gamma = E - \tfrac{1}{2}Mv^2 - MvV$$

$$= E - E_R - E_D \qquad (1.4)$$

The γ-ray is thus deficient in energy by a recoil kinetic energy ($E_R = \frac{1}{2}Mv^2$) which is independent of the initial velocity V, and by a thermal or Doppler energy ($E_D = MvV$) which depends on V and can therefore be positive or negative.

Momentum must also be conserved in the emission process. The momentum of the photon is E_γ/c where c is the velocity of light, so that

$$MV = M(V + v) + E_\gamma/c \qquad (1.5)$$

and the recoil momentum is $Mv = -E_\gamma/c$. Hence the recoil energy is given by

$$E_R = \frac{E_\gamma^2}{2Mc^2} \qquad (1.6)$$

and depends on the mass of the nucleus and the energy of the γ-ray. However, the Doppler energy E_D is dependent on the thermal motion of the nucleus, and will therefore have a distribution of values which is temperature dependent. A mean value, E_D, can be defined which is related to the mean kinetic energy per translational degree of freedom, $\overline{E_k} \simeq \frac{1}{2}kT$, by

$$\overline{E_D} = 2\sqrt{(\overline{E_k}E_R)} = E_\gamma\sqrt{\frac{2\overline{E_k}}{Mc^2}} \qquad (1.7)$$

where k is Boltzmann's constant and T is the absolute temperature.

As a result, the statistical distribution in energy of the emitted γ-rays is displaced from the true excited-state energy by $-E_R$ and broadened by E_D into a Gaussian distribution of width $2\overline{E_D}$. The distribution for absorption has the same shape but is displaced by $+E_R$. This is illustrated schematically in Fig. 1.1, and the order of magnitude of E_R and E_D is indicated in Table 1.1. Nuclear resonant absorption (which in practice can only be observed following an emission) will only have a significant probability if the emission and absorption energy distributions overlap strongly. The recoil and thermal broadening clearly prevent this. It is possible to compensate partially for E_R by moving the emitter towards the observer at a very large (supersonic) velocity, or to increase the Doppler broadening by raising the temperature. Both result in only a marginal increase in the resonant overlap. Furthermore, the intrinsic resolution in the energy of the photon has been degraded to about 1 in 10^7.

It should be noted that these equations are not peculiar to nuclear processes and apply equally well to atomic absorption. However, in the latter case the low energy of the transition results in the recoil energy being significantly less than the thermal broadening. Consequently the overlap for absorption is large and the effects of recoil may be ignored.

1.2 The Mössbauer effect

The Mössbauer effect is unique in that it provides a means of *eliminating* the destructive effects of the recoil and thermal energies. The key to the problem lies in the behaviour of the recoiling nucleus when it is no longer isolated (as is implicit in the preceeding discussion), but instead is fixed in a crystal lattice. As can be seen from Table 1.1, the recoil energy is much less than the chemical binding energy, but is similar in magnitude to the lattice-vibration phonon energies. If the recoil energy is transferred directly to

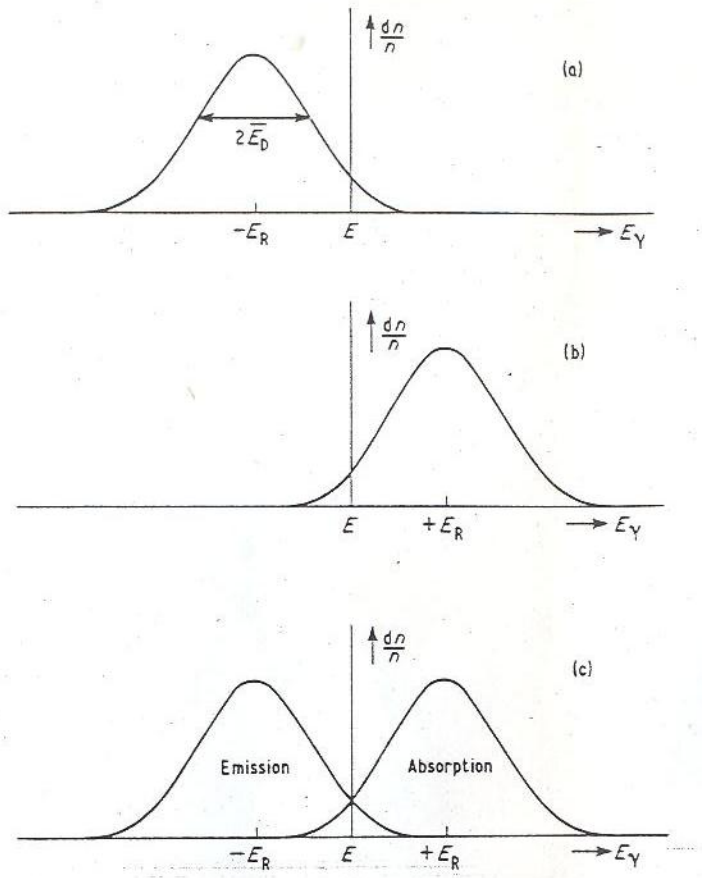

Fig. 1.1 The statistical distribution in the γ-ray energy for (a) emission, (b) absorption, and (c) the resonant overlap for successive emission and absorption.

vibrational energy, then the γ-ray energy is still degraded. However, the phonon energies are quantized, and the recoil energy can only be transferred to the lattice if it corresponds closely to an allowed quantum jump.

The simplest mathematical treatment is one in which the vibrational characteristics correspond to an Einstein solid with one vibrational frequency, ω. Transfer of energy to the lattice can only take place in integral multiples of $\hbar\omega$ $(0, \pm\hbar\omega, \pm 2\hbar\omega, \ldots)$. If the recoil energy E_R is less than $\hbar\omega$, then either zero or one unit $(\hbar\omega)$ of vibrational energy may be transferred to the lattice. It has been

shown by Lipkin [4] that when many emission processes are considered, the *average* energy transferred per event must exactly equal E_R. If a fraction, f, of emission events result in no transfer of energy to the lattice (zero-phonon transitions), and a fraction $(1-f)$ transfer one phonon of energy $\hbar\omega$, then

$$E_R = (1-f)\hbar\omega$$

or

$$f = 1 - E_R/(\hbar\omega) \tag{1.8}$$

In a zero-phonon emission, the whole crystal rather than a single nucleus recoils. Equations (1.6) and (1.7) for E_R and $\overline{E_D}$ contain the reciprocal mass, $1/M$. If the mass M is increased to that of a crystallite containing perhaps 10^{15} atoms, then both the recoil energy and the Doppler broadening become very small and much less than Γ. Hence zero-phonon transitions are referred to as *recoilless*. In any real solid there will be a wide range of lattice frequencies, but fortunately it is very difficult to excite the low frequencies and there is still a significant fraction of nuclear events in which the γ-ray energy is not degraded.

To summarize, the Mössbauer effect is the resonant emission or absorption of γ-rays *in a solid matrix* without degradation by recoil or thermal broadening, and it gives an energy distribution dictated by the Heisenberg uncertainty principle.

The parameter f is known as the recoilless or recoil-free fraction, and to increase the relative strength of the recoilless resonant process it is important that f be as large as possible. On a more quantitative theory [5, 6] it is possible to relate f to the vibrational properties of the crystal lattice by

$$f = \exp\left(-\frac{E_\gamma^2 \langle x^2\rangle}{(\hbar c)^2}\right) \tag{1.9}$$

where $\langle x^2\rangle$ is the mean-square vibrational amplitude of the nucleus in the direction of the γ-ray. From the form of the exponent, f will only be large for a tightly bound atom with a small mean-square displacement, and for a small value of the γ-ray energy, E_γ. For

the latter reason the highest energy for which a Mössbauer resonance is known is 187 keV in ^{190}Os.

The precise form of $\langle x^2 \rangle$ depends on the vibrational properties of the lattice. In any real solid these are usually complex and adequate models are not available. However, it is instructive to consider the behaviour predicted [6] by the Debye model, which embodies a continuum of vibrational frequencies in the harmonic oscillator approximation following the distribution $N(\omega)$ = constant $\times \omega^2$, up to a maximum value of ω_D. A characteristic temperature θ_D is defined by $\hbar\omega_D = k\theta_D$ and is known as the Debye temperature. The final expression obtained is

$$f = \exp\left\{-\frac{6E_R}{k\theta_D}\left[\frac{1}{4} + \left(\frac{T}{\theta_D}\right)^2 \int_0^{\theta_D/T} \frac{x\,dx}{e^x - 1}\right]\right\} \qquad (1.10)$$

From the form of the equation it can be seen that f is large when θ_D is large (a strong lattice) and when the temperature T is small. This decrease in f with rise in temperature follows in general from equation (1.9), in that thermal energy will increase the amplitude of vibration of the nucleus, but the precise form of the temperature dependence can only be predicted using a model for the lattice vibrations. This problem is discussed in more detail in Chapter 6.

It should be noted that although the recoilless fraction can be increased by lowering the temperature there is a limiting value at absolute zero which is still less than unity. For instance, from equation (1.10) when $T = 0$

$$f_{T=0} = \exp\left(-\frac{3E_R}{2k\theta_D}\right) \qquad (1.11)$$

which still depends on E_R and θ_D.

In summary, recoilless emission or absorption is optimized for a low-energy γ-ray with the nucleus strongly bound in a crystal lattice at low temperature.

1.3 The Mössbauer spectrum

Having determined the conditions under which recoilless resonant absorption can occur, it is possible to devise a simple experiment to demonstrate the effect. A solid matrix containing the excited nuclei of a suitable isotope is used as the source of γ-rays. It is placed alongside a second matrix of identical material containing the same isotope in its ground state, which becomes the absorber. The intensity of the γ-radiation transmitted through the absorber is measured as a function of temperature. If there is no resonant absorption, the counting rate is independent of temperature. If resonant absorption occurs, then there should be a decrease in the transmission as the temperature is lowered, and the recoilless fraction increases. The resonantly absorbed γ-rays are effectively lost from the transmitted beam of radiation. Some are re-emitted in a random direction (i.e. resonant fluorescence), while others are lost by an internal conversion process during decay of the excited level (see p.11).

Although this was the experiment first used by R. L. Mössbauer, it is not particularly useful. The method which he also pioneered and has now been adopted exclusively is far more subtle. The definition of the energy of the γ-ray emitted by the source in a recoilless Mössbauer event is about 1 in 10^{12}–10^{13}, and corresponds conveniently to the Doppler energy shifts produced by small movements. If the source and absorber are in relative motion with a velocity v, then the effective value of E_γ 'seen' by the absorber differs from the true energy by a small Doppler shift energy of $\epsilon = (v/c)E_\gamma$. In the event that v is zero, the emission and absorption profiles completely overlap and the absorption is at a maximum. Any increase or decrease in v can only decrease the overlap. If v is very large (of either sign) there will be no overlap and no absorption. It therefore follows that a record of transmission as a function of the velocity v will show an 'absorption spectrum'. This is illustrated schematically in Fig.1.2. By convention a positive velocity is taken to be a closing velocity as this represents an increase in the apparent energy of the photon arriving at the absorber.

The lineshape of the absorption is derived simply from the Heisenberg uncertainty in the energy. The distribution of the recoilless source radiation is given by

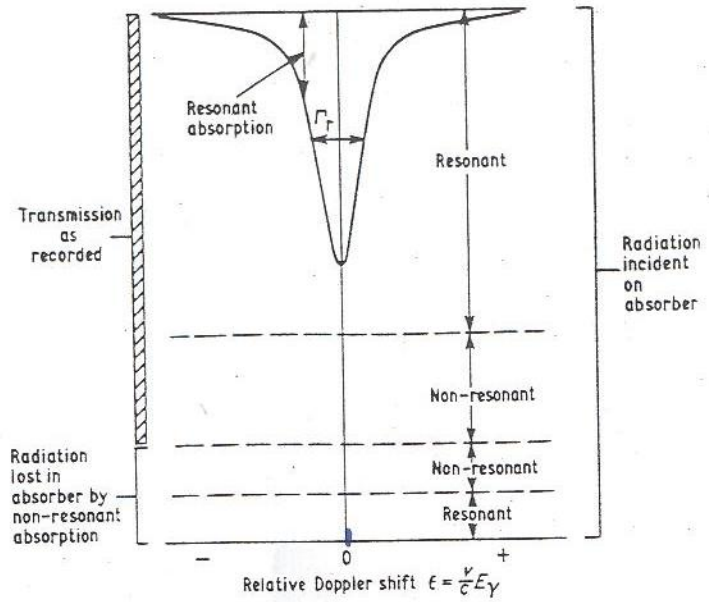

Fig. 1.2 A schematic representation of a Mössbauer transmission spectrum produced by Doppler scanning.

$$N(E)\mathrm{d}E = \frac{f\Gamma}{2\pi}\,\frac{\mathrm{d}E}{(E-E_\gamma)^2+(\Gamma/2)^2} \tag{1.12}$$

where $N(E)$ is the probability of the energy being between E and $E + \mathrm{d}E$, f is the recoilless fraction of the source and Γ is the Heisenberg width. This function which is usually referred to as the Lorentzian distribution has a maximum value at $E = E_\gamma$. The cross-section for resonant absorption, $\sigma(E)$, is similarly expressed [6, 7] as

$$\sigma(E) = \sigma_0\,\frac{(\Gamma/2)^2}{(E-E_\gamma)^2+(\Gamma/2)^2} \tag{1.13}$$

where σ_0 is a nuclear constant called the absorption cross-section given by

$$\sigma_0 = 2\pi(\hbar c/E_\gamma)^2\,\frac{2I_e+1}{2I_g+1}\,\frac{1}{1+\alpha} \tag{1.14}$$

where I_e and I_g are the nuclear spin quantum numbers of the excited and ground states and α is the internal conversion coefficient of the γ-ray [Note: γ-emission does not always lead to an observable γ-ray. In a proportion of events an atomic s-electron is ejected instead in a process known as internal conversion. α is defined as the ratio of the number of conversion electrons to the number of γ-ray photons emitted. Values for σ_0 are often quoted in units of barns (1 barn = 10^{-24} cm^2 = 10^{-28} m^2)]. For σ_0 to be large, both E_γ and α should be small.

In any real absorber of finite thickness the resonant absorption is in direct competition with other non-resonant processes such as Compton scattering. A general evaluation of the integrated absorption intensity or 'transmission integral' is extremely difficult, but to a first approximation the basic behaviour is comparatively simple [8]. The recorded absorption spectrum for infinitely thin sources and absorbers has a Lorentzian distribution with a width at half-height of $\Gamma_r = 2\Gamma$. For an absorber of finite thickness containing t_a resonant atoms per unit area of cross-section and with a recoilless fraction of f_a, an 'effective thickness' is usually defined by the dimensionless parameter $T_a = f_a\sigma_0 t_a$. The absorption shape approximates very closely to Lorentzian but with a broadened width Γ_r given by

$$\Gamma_r/\Gamma \simeq 2 + 0.27T_a \tag{1.15}$$

provided that $T_a < 5$; i.e. the line broadens with an initially linear dependence on thickness. Self-resonance in the source matrix results in an additional line broadening which is approximately independent of absorber thickness.

The probability that any given photon will be resonantly absorbed can be enhanced by increasing the thickness T_a. However, the intensity of the incident γ-ray beam is also strongly attenuated by conventional non-resonant absorption processes, and this places an upper limit on the value of T_a which can be used effectively. The absorption may be defined in terms of the transmitted intensity at the resonant maximum (I_0) and the transmitted intensity at a large Doppler velocity where the absorption is zero (I_∞) by

$$A = (I_\infty - I_0)/I_\infty \tag{1.16}$$

It has been evaluated [8] to be

$$A = f[1 - e^{-T_a/2} J_0(iT_a/2)] \tag{1.17}$$

where f is the recoilless fraction of the source and $J_0(x)$ is a zero-order Bessel function. The value of A/f as a function of T_a is plotted in Fig.1.3, and illustrates how the absorption shows a saturation behaviour with increasing thickness. The effects of non-resonant attenuation combined with more practical problems concerning background radiation levels make it advisable to use the smallest value of T_a which gives an adequate absorption. In practice there is usually an optimum range of absorber thickness for each isotope which is quickly derived from experience.

One of the unfortunate problems which arises is that it is difficult to determine absolute values for the recoilless fractions f and f_a directly from the absorption intensity without tedious and difficult experimentation. However, in the majority of applications accurate values for these parameters are not required.

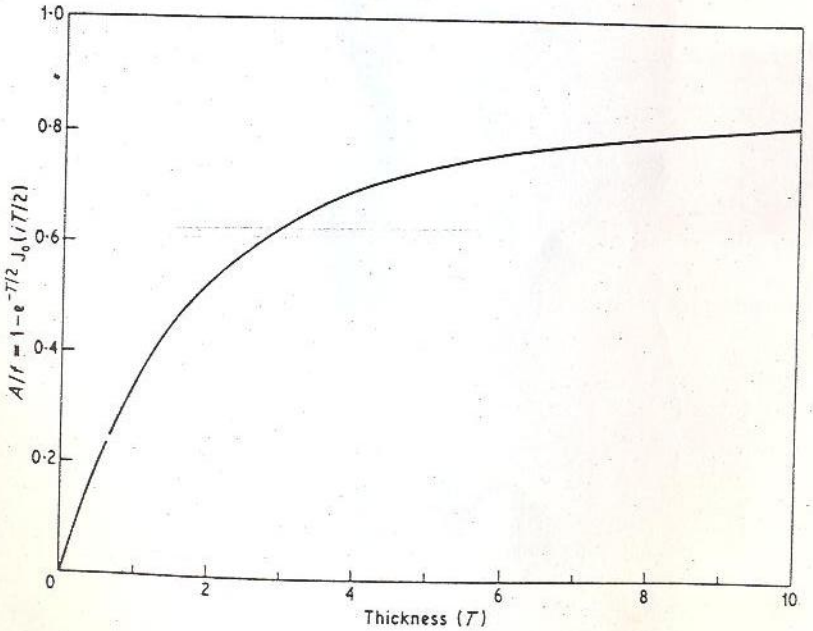

Fig. 1.3 The function $A/f = 1 - e^{-T/2} J_0(iT/2)$ showing how the absorption, A, shows a saturation behaviour with increasing thickness, T.

1.4 The Mössbauer spectrometer

The Mössbauer spectrum is a record of the transmission of resonant γ-rays through an absorber as a function of the Doppler velocity with respect to the source. It is therefore quite simply a record of transmission as a function of the energy of the incident radiation. The major difference from other forms of transmission spectroscopy is that the hazard to health in using high-energy radiation, combined with the high cost of producing the radioisotopes, necessitates the use of relatively low photon flux-densities. In consequence, much longer counting times are required to achieve a given resolution (hours rather than minutes). The statistics of the random counting predicts that the standard deviation in N registered events is $\sqrt{N}$: thus the standard deviation in 10 000 counts is 1% and in 1 000 000 counts is 0.1% of the total count. A prospective gain in resolution must be balanced against the longer experimental time involved, which brings with it the problem of long-term reproducibility in the measuring equipment. To double the resolution requires four times the counting time, and makes it imperative to obtain as large a percentage absorption as possible.

The measurement of a Mössbauer spectrum is almost exclusively carried out by repetitively scanning the whole velocity range required, thereby accumulating the whole spectrum simultaneously, and allowing continuous monitoring of the resolution. This can be achieved electromechanically, and a typical modern Mössbauer spectrometer is illustrated schematically in Fig.1.4. The following description is a brief outline of the major principles involved. For a more detailed account of instrumentation and experimental methods the reader is referred to a recent review by Kalvius and Kankeleit [9].

The major component is a device known as a multichannel analyser which can store an accumulated total of γ-counts, using binary memory storage like a computer, in one of several hundred individual registers known as channels. Each channel is held open in turn for a short time interval of fixed length, which is derived from a very stable constant-frequency clock device. Any γ-counts registered by the detection system during that time interval are added to the accumulated total already stored in the channel. The sequential accessing of the channels is completed in about 1/20 of a second, and is repeated *ad infinitum*.

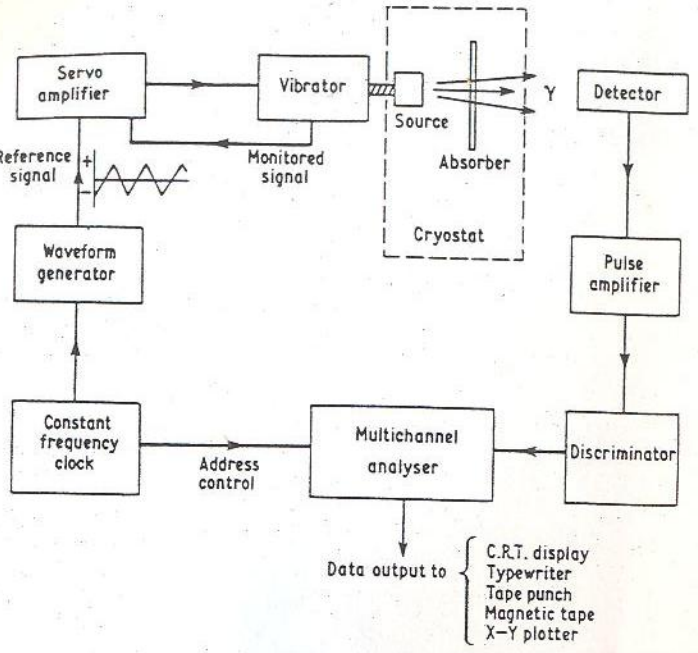

Fig. 1.4 A schematic arrangement for a Mössbauer spectrometer.

The timing pulses from the clock may also be used to synchronize a voltage waveform, which is used as a command signal to the servo-amplifier controlling an electromechanical vibrator. The latter moves the source relative to the absorber. A waveform, with a voltage increasing linearly with time, imparts a motion with a constant acceleration in which the drive shaft and the source spend equal time intervals at each velocity increment. The multichannel analyser and the drive are synchronized so that the velocity changes linearly from $-v$ to $+v$ with increasing channel number. In this way the source is always moving at the same velocity when a given channel is open.

The γ-ray detection system is conventional. A scintillation counter, gas proportional counter, or lithium-drifted germanium detector may be used according to circumstances [10]. The pulses from the detector are amplified, passed through a discriminator which rejects most of the non-resonant background radiation, and finally are fed to the open channel address.

The geometric arrangement of the source, absorber and detector is important. A γ-ray emitted along the axis of motion of the source has a Doppler shift relative to the absorber of $E_\gamma v/c$, but any γ-ray which travels to the detector along a path at an angle θ to this axis has an effective Doppler shift of only $E_\gamma v\cos\theta/c$. This 'cosine-effect' of solid-angle will therefore cause a spread in the apparent Doppler energy of the γ-rays and hence line broadening [11]. The effect can be reduced by maintaining an adequate separation between the source and detector, or by collimation.

The velocity range required to completely encompass the absorption is usually less than ± 10 mm s^{-1}, so that the overall displacement of the source during a scan is barely discernible. Absolute calibration of the drive is not easy, but can be achieved by mounting a diffraction grating or mirror on the shaft as part of an interferometer. For most purposes it is more convenient to rely on an internal standard. As will be seen in the next chapter, it is possible for an absorber to show more than one resolved absorption line. If such a material is chemically reproducible and stable, and the lines are measured on an instrument with absolute calibration, it can then be used in other laboratories to establish the velocity amplitude and linearity of uncalibrated instruments. For example, it is common practice to use a magnetic α-iron foil which has six lines as a calibrant for ^{57}Fe work, and to quote all measurements of velocity relative to the centroid of this reference spectrum.

Very few Mössbauer resonances are easy to record at room temperature, the main exceptions being ^{57}Fe and ^{119}Sn, and in many instances it is necessary to cool at least the absorber, and sometimes the source as well, to increase the recoilless fractions. Because the source is moving, this is not without its difficulties. There is also the possibility that some of the hyperfine interactions (to be described in Chapter 2) are temperature dependent. For this reason alone, low-temperature measurements have become popular [9]. Numerous commercial cryostats are now available, the commonly used refrigerants being liquid nitrogen for temperatures down to 78 K and liquid helium down to 4.2 K. Cryostats with a fully-variable temperature control are also used, particularly in the study of phase transitions. In some applications it is desirable to apply a large external magnetic field to the absorber, and superconducting magnet installations are available which can produce magnetic flux densities of up to 10T.

Although this discussion has been weighted in favour of using a

transmission experiment to observe resonant absorption, it is also possible to detect resonant fluorescence by a scattering experiment. The resonant absorption event may be recorded by detecting the scattered γ-ray on de-excitation (alternatively, if the internal conversion coefficient α is large, the conversion-electron or X-ray produced may be registered). This has the advantage that non-resonant radiation from the source is not recorded, and the major remaining contributions to the radiation background are scattered higher-energy γ-rays and non-resonant Rayleigh scattering. The main disadvantages are that the intensity of the scattered radiation is very weak, and the large solid geometry requirement for a high count rate results in broadening of the Mössbauer line. A further problem, which may arise if scattered γ-rays are counted, is the possibility of anomalous effects dependent on the scattering angle. These are due to interference between resonant Mössbauer scattering and the non-resonant Rayleigh scattering [12] and to diffraction [13].

The principal application of scattering experiments is in the study of surface phenomena, and examples of this are given in Chapter 9.

1.5 Mössbauer isotopes

Several requirements can be formulated which must be fulfilled if there is to be an easily observable Mössbauer resonance:

(1) The energy of the γ-ray must be between 10 and 150 keV, preferably less than 50 keV, because the recoilless fraction f and resonant cross-section σ_0 both decrease as E_γ increases. This is the main reason why no resonances are known for isotopes lighter than ^{40}K. The γ-transitions in light nuclei are usually very energetic

(2) The half-life of the first excited state which determines Γ should be between about 1 and 100 ns. If $t_{1/2}$ is very long, then Γ is so narrow that mechanical vibrations destroy the resonance condition, and if $t_{1/2}$ is very short then Γ will probably be so broad as to obscure any useful hyperfine effects.

(3) The internal conversion coefficient α should be small (<10) so that there is a good probability of detecting the γ-ray.

(4) A long-lived precursor should exist which can populate the required excited level. This usually means an isotope which decays by β-decay, electron capture, or isomeric transition. Although

some experiments have been done with energetic nuclear reactions *in situ* such as Coulombic excitation or (d, p) reactions, these methods are not applicable to routine measurements.

(5) The ground-state isotope should be stable and have a high natural abundance so that isotopic enrichment of absorbers is unnecessary.

Despite these restrictions, a Mössbauer resonance has been recorded in 100 transitions of 83 different isotopes in 44 elements, the majority of the heavy elements in fact. These are listed at the end of the book. However, many of these resonances can only be recorded with difficulty at the present time. Some of the more useful resonances, many of which are illustrated with examples in later chapters, are listed in Table 1.2. Some of their nuclear properties are also given, including the nuclear spin states I_g and I_e and their parity, and the internal conversion coefficient α.

The most popular Mössbauer resonance is undoubtedly the 14.41-keV γ-transition in ^{57}Fe, and the decay scheme for the ^{57}Co parent is shown in Fig.1.5, together with the decay schemes for the ^{119}Sn, ^{129}I and ^{193}Ir resonances. The conveniently long-lived ^{57}Co nucleus decays by electron-capture with high efficiency to the 136.32-keV level of ^{57}Fe, from whence 85% of the decays proceed to the 14.41-keV level. The lifetime of this state is 99.3 ns, giving a Heisenberg width of $\Gamma_\tau = 0.192$ mm s^{-1} in the Mössbauer resonance. The large value of α for this level (8.17) unfortunately reduces the source efficiency to less than 10%, but the γ-ray is well resolved from the two higher energy γ-rays and the 7-keV X-rays produced by internal conversion. Although the natural abundance of ^{57}Fe is only 2.19%, the absorption cross-section of $\sigma_0 = 2.57 \times 10^{-18}$ cm^2 is unusually large, and results in a satisfactory resonance at room temperature. Metals and refractory materials can give an acceptable absorption even above 1000 K, although organometallic compounds with a low effective Debye temperature are more effective when cooled.

One of the most important experimental aspects is in the choice of a source matrix. It is very desirable to have a high recoilless fraction and a single emission line unbroadened by hyperfine interactions. The best choice of host matrix is usually a high-melting metal or a refractory oxide of cubic structure; for example the most popular host for ^{119m}Sn is the oxide $BaSnO_3$, and ^{57}Co is usually diffused into a metal, such as palladium, platinum or rho-

Table 1.2 Nuclear parameters for selected Mössbauer transitions

Isotope	E_γ/keV	Γ_τ/ (mm s^{-1})	I_g	I_e	α	Natural abundance (%)	Nuclear decay*
^{57}Fe	14.41	0.192	1/2−	3/2−	8.17	2.17	^{57}Co(EC 270 d)
^{61}Ni	67.40	0.78	3/2−	5/2−	0.12	1.25	^{61}Co(β^-99 m)
^{99}Ru	90	0.147	5/2+	3/2+	–	12.63	^{99}Rh(EC 16 d)
^{119}Sn	23.87	0.626	1/2+	3/2+	5.12	8.58	^{119m}Sn(IT 250 d)
^{121}Sb	37.15	2.1	5/2+	7/2+	~10	57.25	^{121m}Sn(β^- 76 y)
^{125}Te	35.48	5.02	1/2+	3/2+	12.7	6.99	^{125}I(EC 60 d)
^{127}I	57.60	2.54	5/2+	7/2+	3.70	100	^{127m}Te (β^-109 d)
^{129}I	27.72	0.59	7/2+	5/2+	5.3	nil	^{129m}Te (β^-33 d)
^{129}Xe	39.58	6.85	1/2+	3/2+	11.8	26.44	^{129}I(β^- 1.7×10^7 y)
^{149}Sm	22.5	1.60	7/2−	5/2−	~12	13.9	^{149}Eu(EC 106 d)
^{151}Eu	21.6	1.44	5/2+	7/2+	29	47.8	^{151}Gd(EC 120 d)
^{161}Dy	25.65	0.37	5/2+	5/2−	~2.5	18.88	^{161}Tb(β^- 6.9 d)
^{169}Tm	8.40	9.3	1/2+	3/2+	220	100	^{169}Er(β^- 9.4 d)
^{182}W	100.10	2.00	0+	2+	3.2	26.4	^{182}Ta(β^- 115 d)
^{189}Os	69.59	2.41	3/2−	5/2−	8.2	16.1	^{189}Ir(EC 13.3 d)
^{193}Ir	73.0	0.60	3/2+	1/2+	~6	61.5	^{193}Os(β^- 31 h)
^{197}Au	77.34	1.87	3/2+	1/2+	4.0	100	^{197}Pt(β^-18 h)
^{237}Np	59.54	0.067	5/2+	5/2−	1.06	nil	^{241}Am (α458 y)

*EC = electron capture, β^- = beta-decay, IT = isomeric transition, α = alpha-decay

dium. However, these were chosen as the result of experience, and the development of a good source is of prime importance in studying a new resonance.

In some instances where the absorption is too weak, a substantial improvement can be obtained by using isotopic enrichment.

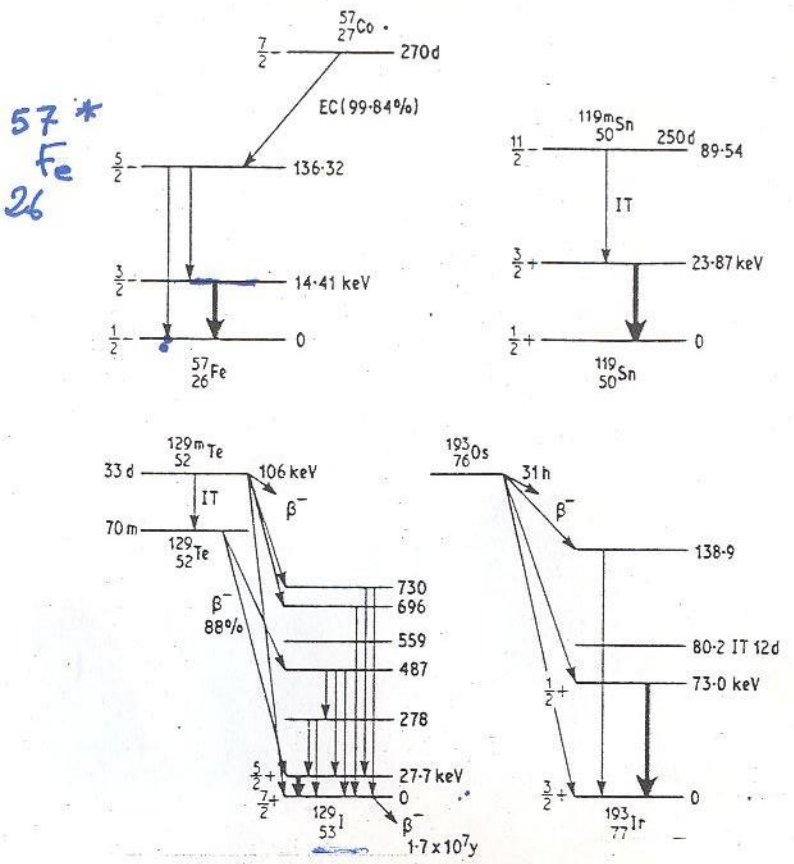

Fig. 1.5 The nuclear decay schemes for the Mössbauer resonances in ^{57}Fe, ^{119}Sn, ^{129}I and ^{193}Ir.

Thus ^{57}Fe has an abundance of only 2.17% in natural iron, but material enriched to 90% can be used in compounds with a very low total iron content (eg. dilute iron alloys or haeme-proteins) to obtain an adequate cross-section for absorption.

1.6 Computation of data

The characteristic digital data comprising a Mössbauer spectrum are in an ideal form for statistical calculations by digital computer. For this reason the multichannel analyser is usually equipped to

output data in a form suitable for input to one of the standard computer peripherals.

Each spectrum comprises N digital values, Y_i, of the number of γ-counts registered at velocities x_i. The statistics of spontaneous radioactive decay processes follow a Poisson distribution [14]. If the mean value of the number of counts recorded in a given time is Y, then the standard deviation in Y is $\sqrt{Y}$. In its simplest form the Mössbauer spectrum comprises a single absorption line which has a Lorentzian shape, and can therefore be specified completely by four parameters; the linewidth, the line position, the intensity of the absorption, and the baseline count for zero absorption. These parameters may always be found by visual inspection, but more precise values, together with their standard deviations, are obtained by computing a least-squares fit to the data. Appropriate starting values of the n parameters are 'guessed' and used to calculate the 'theoretical' value of data point i to be $A_i(n)$. The discrepancy between the observed data and the assumed model can be represented by the weighted sum of the squares of the differences

$$F = \sum_{i=1}^{N} \left\{ \frac{[Y_i - A_i(n)]^2}{Y_i} \right\} \qquad (1.18)$$

This expression can be used as a 'goodness-of-fit' function and minimized by standard mathematical routines to give the best values of the n variables. The function F has N-n degrees of freedom and the properties of a chi-squared distribution at the minimum [14]; it may be related to the probability that the theoretical model is a valid description of the data, and in conjunction with statistical tables [15] its value indicates the degree of confidence to be placed on the final answers. For example, a computed fit to data with 400 degrees of freedom is within the 25–75% confidence limits of the χ^2 distribution if $380 < F < 419$, and within the 5–95% limits if $355 < F < 448$. A value outside these limits is generally indicative of either faulty data or an inappropriate theoretical model.

The most commonly used theoretical function is a summation of Lorentzian lines, but the same basic principles are valid for any function which correctly describes the data. However, one word

of caution must be given. A good fit to data is *not* unambiguous proof that the theoretical function is the correct one. In a complicated spectrum it is quite feasible to fit a function which has no physical significance. The final data analysis *must* be compatible with other scientific evidence, and inevitably there will be instances where it is not possible to distinguish between alternative hypotheses.

References

[1] Mössbauer, R. L. (1958) *Z. Physik*, 151, 124.
[2] Kuhn, W. (1929) *Phil. Mag.*, 8, 625.
[3] Metzger, F. R. (1959) *Progr. Nuclear Phys.*, 7, 54.
[4] Lipkin, H. J. (1960) *Ann. Phys.*, 9, 332.
[5] Petzold, J. (1961) *Z. Physik*, 163, 71; Wisscher, W. M. (1960) *Ann. Phys.*, 9, 194.
[6] Frauenfelder, H. (1962) *The Mössbauer Effect*, W. A. Benjamin Inc., N.Y.
[7] Jackson, J. D. (1955) *Can. J. Phys.*, 33, 575.
[8] Margulies, S. and Ehrman, J. R. (1961) *Nuclear Instr. Methods*, 12, 131.
[9] Kalvius, G. M. and Kankeleit, E. (1972) Recent improvements in instrumentation and methods of Mössbauer spectroscopy. In *Mössbauer Spectroscopy and its Applications*, International Atomic Energy Agency, Vienna, p.9.
[10] (1965) *Alpha-, beta-, and gamma-ray spectroscopy* Vol.1, ed. K. Siegbahn, North-Holland, Amsterdam.
[11] Riesenman, R., Steger, J. and Kostiner, E. (1969) *Nuclear Instr. Methods*, 72, 109.
[12] Black, P. J., Longworth, G. and O'Connor, D. A. (1964) *Proc. Phys. Soc.*, 83, 925.
[13] Black, P. J. and Duerdoth, I. P. (1965) *Proc. Phys. Soc.*, 84, 169.
[14] Mulholland, H. and Jones, C. R. (1968) *Fundamentals of Statistics*, Butterworths, London.
[15] Beyer, W. H. (editor), (1968) *Handbook of Tables for Probability and Statistics*, 2nd edition. The Chemical Rubber Co., Cleveland.

CHAPTER TWO

Hyperfine Interactions

In Chapter 1 it was shown that the Mössbauer spectrum is a record of the intensity of a transmitted γ-ray beam as a function of the Doppler velocity between the source and absorber. The resonant absorption line has a Lorentzian shape of width Γ_γ and is centred at zero relative velocity between source and absorber. The practical application of this measurement would be limited were it not for the fact that the energies of the nuclear states are weakly influenced by the chemical environment. It is possible to detect these extremely small effects because of the high definition (better than 1 in 10^{12}) of the γ-ray energy.

There are three principal interactions to consider. These are:

(1) A change in the electric monopole or Coulombic interaction between the electronic and nuclear charges, which is caused by a difference in the size of the nucleus in its ground and excited states. This is seen as a shift of the absorption line away from zero velocity and is variously known as the chemical isomer shift, isomer shift, or centre shift, and designated by the symbol δ.

(2) A magnetic dipole interaction between the magnetic moment of the nucleus and a magnetic field. The origin of the latter may be intrinsic or extrinsic to the atom. The result is a multiplet line structure in the spectrum known as magnetic hyperfine splitting.

(3) An electric quadrupole interaction between the nuclear

quadrupole moment and the local electric field gradient tensor at the nucleus. This also results in a multiple-line spectrum.

Magnetic hyperfine interactions were first observed by Pound and Rebka in 1959 [1], and the chemical isomer shift and quadrupole interactions by Kistner and Sunyar in 1960 [2]. At first sight the rapid development of Mössbauer spectroscopy from then onwards seems extraordinary, but it should be realized that most of the underlying theory was already available. The chemical isomer shift is similar in origin to the isotope shift in atomic spectra. Electric quadrupole interactions are the basis of nuclear quadrupole resonance, while the magnetic dipole interactions together with the theory of time-dependent processes were familiar in nuclear magnetic resonance and electron spin resonance spectroscopy.

All three effects may occur together, but only the magnetic and quadrupole interactions are directional and thus have a complicated interrelationship. The chemical isomer shift behaves independently of the other two interactions, and is conveniently considered first.

Although this chapter emphasizes the ways in which the hyperfine interactions of the nucleus are used to investigate the chemical environment, it should be noted that many of the early measurements on each Mössbauer resonance were made to obtain values for the nuclear parameters. For example, although the spin, magnetic moment, and quadrupole moment are usually known for the ground state of the nucleus, this is not necessarily the case for an excited state. It has often been necessary to determine one or more of these parameters from the hyperfine interactions in appropriately selected compounds.

2.1 The chemical isomer shift

In most instances it is adequate to consider the Coulombic interaction between the electrons and the nucleus as if the latter were a point charge. This assumption is made for example in solving the Schrödinger wave equation for the electronic structure of the atom. Such a simplification predicts that there will be no change in the Coulombic interaction energy when the nuclear excited state decays to the ground state. However, the nucleus does have a finite size which may change fractionally during the transition. It must also be realized that an *s*-electron wavefunction has a finite value

inside the nuclear radius, and is directly responsible for the change in electrostatic energy observed.

The integrated Coulombic energy for an electron of charge $-e$ moving in the field of a point nucleus of charge $+Ze$ is given by

$$E_0 = -\frac{Ze^2}{4\pi\epsilon_0}\int_0^\infty \Psi^2 \frac{d\tau}{r} \qquad (2.1)$$

where ϵ_0 is the permittivity of a vacuum, r is the radial distance, and $-e\Psi^2$ is the charge density of the electron in volume element $d\tau$. If the nucleus is spherical with a radius R, then equation (2.1) is valid for $r > R$, but overestimates E_0 for $r < R$. It is possible to calculate an approximate correction, W, by assuming a model for the proton charge density within the nucleus [3]. If this is taken to be uniform, and certain simplifying approximations are made in the mathematics, the comparatively simple expression obtained is

$$W = \frac{1}{10\epsilon_0} Ze^2R^2|\Psi_s(0)|^2 \qquad (2.2)$$

where $|\Psi_s(0)|^2$ is the non-relativistic Schrödinger wavefunction at $r = 0$.

If the nucleus changes its radius by a small increment δR during its transition from the excited state to the ground state, there will be a simultaneous change in electrostatic energy given by

$$\Delta W = \frac{1}{5\epsilon_0} Ze^2R^2 \frac{\delta R}{R} |\Psi_s(0)|^2 \qquad (2.3)$$

The value of $\delta R/R$ is characteristic of each transition, but is typically of the order of 10^{-4} and may be of either sign. A positive sign means that the nucleus shrinks on de-excitation. The Mössbauer experiment compares the difference in energy between the nuclear transitions in the source and absorber, so that the chemical isomer shift as observed is given by

$$\delta = \frac{1}{5\epsilon_0} Ze^2R^2 \frac{\delta R}{R} (|\Psi_s(0)_{\text{absorber}}|^2 - |\Psi_s(0)_{\text{source}}|^2) \qquad (2.4)$$

This can then be related quite simply to the measured shift in Doppler velocity units, v, by $v = (c/E_\gamma)\delta$. (The customary symbol for the chemical isomer shift, δ, is not to be confused with the change in nuclear radius, δR).

Equation (2.4) can be seen to be the product of a chemical term (the electron density at $r = 0$) and a nuclear term (the change in nuclear radius). The latter is a constant for a particular transition, and thus it is possible to study relative changes in electron density directly. Equations similar to (2.4) are sometimes used which express the nuclear radius as a mean-square value to indicate that it is not necessarily spherical, but these may be converted to the expression above by using the relationships $\delta\langle R^2\rangle/\langle R^2\rangle = 2\delta R/R$ and $\langle R_e^2\rangle - \langle R_g^2\rangle = \frac{5}{5}R^2(\delta R/R)$. For chemical applications it is often sufficient to compare chemical isomer shift values using the simplified expression

$$\delta = \text{constant} \times (|\Psi_s(0)_A|^2 - |\Psi_s(0)_B|^2) \qquad (2.5)$$

where A and B are two different chemical environments of which B is either the source matrix or a reference absorber.

It is important to realize that $|\Psi_s(0)|^2$ is the *s*-electron density *at the nucleus*, and not the *s*-electron occupation in the formal chemical sense. If $\delta R/R$ is positive, a positive value of the chemical isomer shift, δ, implies that the *s*-electron density at the nucleus in A is greater than in B. $|\Psi_s(0)|^2$ includes contributions from all the occupied *s*-electron orbitals in the atom, but is naturally more sensitive to changes which take place in the outer valence shells. Although the values of $|\Psi(0)|^2$ for *p*-, *d*- and *f*-electrons are zero, these orbitals nevertheless do have a significant *indirect* interaction with the nucleus via interpenetration shielding of the *s*-electrons. For example a $3d^54s^1$ configuration will have a larger value of $|\Psi_s(0)|^2$ than $3d^64s^1$ because in the latter case the extra *d*-electron shields the 4*s*-electron from the nucleus.

In a number of instances a Mössbauer resonance can be observed for two or more transitions to the same ground state, or for several isotopes of the same element. The chemical isomer shifts of two

different resonances in the same series of compounds should be interrelated purely by the difference in $\delta R/R$, and this appears to be the case. An interesting illustration is provided by the ^{127}I and ^{129}I spectra of $Na_3H_2IO_6$ shown in Fig.2.1. The source matrix was zinc telluride in each case but containing ^{127m}Te and ^{129m}Te respectively [4]. These isotopes β-decay to populate the 57.6-keV level of ^{127}I and the 27.7-keV level of ^{129}I. The absorptions occur at positive and negative velocities because $\delta R/R$ is negative in ^{127}I and positive in ^{129}I, while the s-electron density at the nucleus is greater in the source than the absorber. The relative magnitudes of the shift also differ because $[\delta R/R(^{127}\mathrm{I})]/[\delta R/R(^{129}\mathrm{I})] = -0.65$. The resonance lines have different widths because $\Gamma_r = 2.54$ mm s^{-1} for ^{127}I and 0.59 mm s^{-1} for ^{129}I.

An accurate calibration of the chemical isomer shift scale for a particular isotope is not without difficulties. The change in nuclear radius, $\delta R/R$, cannot be determined independently of the chemical environment, which means that the electron density $|\Psi_s(0)|^2$, has to be estimated by molecular orbital methods in at least two compounds before a value for $\delta R/R$ can be obtained. Some of the problems which this creates are discussed in Chapter 4.

The observed line-shift is not entirely caused by the chemical isomer shift as described above. There is another generally smaller contribution termed the second-order Doppler shift, which was first observed by Pound and Rebka in 1960 [5]. The emitting or absorbing nucleus is not stationary but is vibrating on its lattice site. The period of vibration is much shorter than the Mössbauer lifetime so that the average displacement and velocity are effectively zero, but the mean-squared values of the velocity, $\langle v^2 \rangle$, are finite.

The relativistic equation for the Doppler effect on the apparent frequency ν of the emitted photon (as recorded at the absorbing nucleus) is

$$\nu = \nu_0 \left(1 - \frac{v}{c}\cos\alpha\right)\left(1 - \frac{v^2}{c^2}\right)^{-1/2} \qquad (2.6)$$

where ν_0 is the frequency for a stationary nucleus, and v is the apparent relative velocity of the emitting nucleus along a direction making an angle α with the γ-ray direction (Note: v is not the velocity along the direction of travel of the γ-ray). For an oscillatory

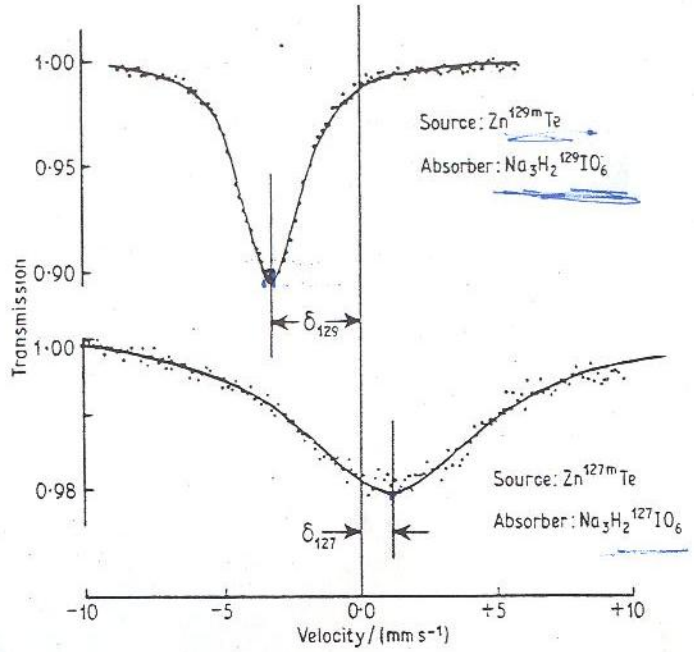

Fig. 2.1 The ^{127}I and ^{129}I spectra of $Na_3H_2IO_6$ showing the smaller linewidth and larger chemical isomer shift of opposite sign for the latter ([4], Fig. 1)

motion the mean value $\langle v \rangle$ is zero so that only the second-order term in $\langle v^2 \rangle$ can influence the Mössbauer resonance. Hence for $v \ll c$

$$\nu \simeq \nu_0 \left(1 + \frac{\langle v^2 \rangle}{2c^2}\right) \qquad (2.7)$$

This gives rise to a shift in the Mössbauer line of

$$\frac{\delta E}{E_\gamma} = \frac{\nu_0 - \nu}{\nu_0} = -\frac{\langle v^2 \rangle}{2c^2} \qquad (2.8)$$

It is obvious that $\langle v^2 \rangle$ increases with rise in temperature. Accordingly, the Mössbauer resonance in an absorber moves to a more negative velocity as the temperature is raised. The second-order Doppler shift contribution to the observed chemical shift is smallest

at absolute zero, but is still finite because of a zero-point motion of the nucleus.

The second-order Doppler shift is often ignored when comparing values of the total observed shift because it always acts in the same sense, but such a comparison should only be made for similar compounds at the same temperature, and small differences regarded as not significant. A more detailed discussion of the second-order Doppler shift will be found in Chapter 6.

2.2 Magnetic hyperfine interactions

The nucleus has a magnetic moment, μ, when the spin quantum number, I, is greater than zero. Its energy is then affected by the presence of a magnetic field, and the interaction of μ with a magnetic flux density of B is formally expressed by the Hamiltonian

$$\mathcal{H} = -\boldsymbol{\mu} \cdot \mathrm{B} = -g\mu_N \mathrm{I} \cdot \mathrm{B} \qquad (2.9)$$

where μ_N is the nuclear magneton ($eh/4\pi m_p = 5.04929 \times 10^{-27}$ A m^2 or J T^{-1}) and g is the nuclear g-factor [$g = \mu/(I\mu_N)$]. Solving this Hamiltonian [6] gives the energy levels of the nucleus in the field to be

$$E_m = -\frac{\mu B}{I} m_z = -g\mu_N B m_z \qquad (2.10)$$

where m_z is the magnetic quantum number and can take the values $I, I-1, \ldots, -I$. In effect, the magnetic field splits the energy level into $2I+1$ non-degenerate equi-spaced sublevels with a separation of $\mu B/I$.

In a Mössbauer experiment there may be a transition from a ground state with a spin quantum number I_g and magnetic moment μ_g to an excited state with spin I_e and magnetic moment μ_e. In a magnetic field, both states will be split according to equations (2.9) and (2.10). Transitions can take place between sub-levels provided that the selection rule $\Delta m_z = 0, \pm 1$ is obeyed [this is called a magnetic dipole (M1) transition; for other selection rules see Section 2.5 on line intensities]. The resultant Mössbauer spectrum contains a number of resonance lines, but is nevertheless symmetrical about the centroid.

A typical example of magnetic hyperfine splitting is illustrated schematically in Fig.2.2, which is drawn to a scale appropriate to ^{119}Sn. For this isotope $I_g = \frac{1}{2}$, $I_e = \frac{3}{2}$, $\mu_g = -1.041\mu_N$ and $\mu_e = +0.67\mu_N$. The change in sign of the magnetic moment results in a relative inversion of the multiplets. The six lines are the allowed $\Delta m_z = 0, \pm 1$ transitions, and the resultant spectrum is indicated in the stick diagram. The lines are not of equal intensity, but the 3:2:1:1:2:3 ratio shown here is often found for example in the ^{57}Fe and ^{119}Sn resonances in randomly oriented polycrystalline samples. A more detailed account of relative line intensities is given later in the chapter.

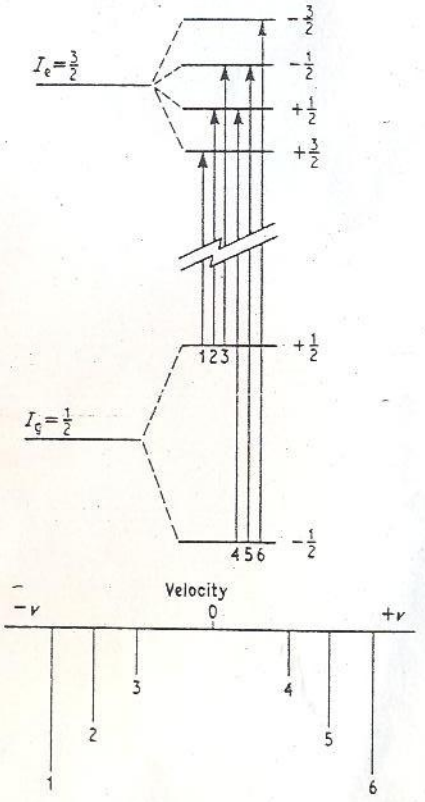

Fig. 2.2 The energy-level scheme and resultant spectrum for magnetic hyperfine splitting of an $I_g = \frac{1}{2} \rightarrow I_e = \frac{3}{2}$ transition. The relative splittings are scaled in accord with the magnetic moments of ^{119}Sn; $\mu_g = -1.041\mu_N$ and $\mu_e = +0.67\mu_N$. The line intensity ratios of 3:2:1:1:2:3 are appropriate to a polycrystalline absorber.

The magnetic field may be applied by an external magnet, or it may be intrinsic to the compound in which case it is usually referred to as an 'internal' field. An unpaired electron in the atomic environment can induce an imbalance in electron spin-density at the nucleus, and thereby generate a local magnetic flux density which can be as large as 100 T. Examples of this may be found in Chapter 5.

The sign of an internal magnetic flux density, B, can sometimes be obtained by applying an additional externally generated magnetic flux density, B_0, with a large magnet. If the resultant flux density in the Mössbauer spectrum has increased to $B + B_0$ by parallel alignment of B with B_0 (i.e. the internal field is parallel to the magnetization) then the sign is positive, whereas a field of $B - B_0$ signifies antiparallel alignment and a negative sign. This method fails if the magnetic anisotropy of the matrix is large enough to prevent rotation of the internal field into the direction of the applied field.

Time-dependent effects such as relaxation are discussed separately in Chapter 6.

2.3 · Electric quadrupole interactions

The electric quadrupole interaction in Mössbauer spectroscopy is very similar to that in nuclear quadrupole resonance spectroscopy [7]. The main difference is that the latter is concerned with radio-frequency transitions *within* a hyperfine multiplet of a ground state nucleus, whereas the former is a γ-ray transition *between* the hyperfine multiplets of the nucleus in its ground and excited states. Only those nuclear states with $I > \frac{1}{2}$ have a nuclear quadrupole moment and hence show a quadrupole hyperfine splitting. In consequence it is often possible to observe a quadrupole interaction in the Mössbauer spectrum which derives from the excited state of the nucleus, even though the ground state has $I_g = 0$ or $I_g = \frac{1}{2}$ and therefore does not give an N.Q.R. signal.

The nuclear quadrupole moment, Q, is a measure of the deviation from spherical symmetry of the nuclear charge. It is expressed by

$$eQ = \int \rho r^2 (3\cos^2\theta - 1)\,d\tau \qquad (2.11)$$

where $+e$ is the charge on the proton, and ρ is the charge density in the volume element $d\tau$ at a distance r from the centre of the nucleus and at an angle θ to the axis of the nuclear spin. The magnitude of Q is often referred to in units of barns (1 barn = 10^{-28} m^2). The sign of Q can be positive or negative according to whether the nucleus is respectively elongated (prolate) or flattened (oblate) along the spin-axis.

The electrostatic potential at the nucleus due to a point charge q at a distance r is given by $V = q/(4\pi\epsilon_0 r)$ where ϵ_0 is the permittivity of a vacuum. The interaction of the nuclear quadrupole moment with the electronic environment is expressed by the Hamiltonian

$$\mathcal{H} = -\frac{1}{6} e\mathbf{Q}\cdot\nabla\mathbf{E} \qquad (2.12)$$

where ∇E represents the electric field gradient at the nucleus (which is the derivative of the electric field, E, and hence the negative of the second derivative of the potential, V). ∇E is a tensor quantity which can be written as

$$\nabla_i E_j = -\frac{\partial^2 V}{\partial x_i \partial x_j} = -V_{ij} \qquad (2.13)$$

$$(x_i, x_j = x, y, z)$$

There are thus nine values of V_{ij} to express ∇E in a Cartesian axis system, x, y, z. A 'principal' axis system may always be defined such that all the V_{ij} terms with $i \neq j$ are zero (the matrix of the tensor is diagonal), leaving the three finite 'principal' values V_{xx}, V_{yy}, and V_{zz}. Furthermore, ΔE is a traceless tensor, so that

$$V_{xx} + V_{yy} + V_{zz} = 0 \qquad (2.14)$$

As a result it is only necessary to specify two parameters to completely describe an electric field gradient tensor in its principal axis sytem. $V_{zz} = eq$ is taken to be the largest value of $|V_{ii}|$, and an asymmetry parameter, η, is defined by

$$\eta = (V_{xx} - V_{yy})/V_{zz} \qquad (2.15)$$

such that $|V_{zz}| > |V_{yy}| \geqslant |V_{xx}|$ and $0 \leqslant \eta \leqslant 1$. The z axis is then referred to as the 'major' axis, and x is the 'minor' axis. The correct assignment of these axes is often obvious from the molecular geometry if the overall symmetry is high; e.g. in a molecule with axial symmetry, the z axis is the symmetry axis. (Note: in an arbitrary axis sytem it is necessary to specify five parameters which may be V_{xx}, V_{xy}, V_{xz}, V_{yy}, and V_{yz}, or alternatively the principal values V_{zz} and η with three angles to specify their orientation with respect to the arbitrary x, y, z axes.)

The Hamiltonian in equation (2.12) is more often written as

$$\mathscr{H} = \frac{eQ}{2I(2I-1)}\left[V_{zz}\hat{I}_z^2 + V_{yy}\hat{I}_y^2 + V_{xx}\hat{I}_x^2\right]$$

$$= \frac{e^2qQ}{4I(2I-1)}\left[3\hat{I}_z^2 - I(I+1) + \eta(\hat{I}_x^2 - \hat{I}_y^2)\right] \qquad (2.16)$$

where $\hat{I}_x$, $\hat{I}_y$ and $\hat{I}_z$ are quantum-mechanical spin operators. A completely general solution of this Hamiltonian is not possible, but exact expressions may be given under certain conditions.

If the electric field gradient tensor has axial symmetry ($\eta = 0$) the energy levels are given by

$$E_Q = \frac{e^2qQ}{4I(2I-1)}\left[3I_z^2 - I(I+1)\right] \qquad (2.17)$$

where the quantum number I_z can take the $2I+1$ values of $I, I-1, \ldots, -I$. If $I = \frac{3}{2}, \frac{5}{2}, \frac{7}{2}$ etc. the energy level is split into a series of Kramers' doublets with $\pm I_z$ states degenerate. An important example is $I = \frac{3}{2}$, which has two energy levels at $+e^2qQ/4$ for $I_z = \pm\frac{3}{2}$ and $-e^2qQ/4$ for $I_z = \pm\frac{1}{2}$. If the symmetry is lower than axial (i.e. when $\eta > 0$), an exact expression can only be given for $I = \frac{3}{2}$, and is

$$E_Q = \frac{e^2qQ}{4I(2I-1)}\left[3I_z^2 - I(I+1)\right](1+\eta^2/3)^{1/2} \qquad (2.18)$$

with energy levels at $\pm(e^2qQ/4)(1+\eta^2/3)^{1/2}$. Values for higher spin states must be calculated numerically.

A Mössbauer transition between states can take place according to the selection rule $\Delta m_z = 0, \pm 1$ for M1 dipole radiation. The most common example is the $I_g = \frac{1}{2} \rightarrow I_e = \frac{3}{2}$ transition in which the ground state with $I_z = \pm\frac{1}{2}$ is unsplit, and the excited state has two levels with $I_z = \pm\frac{3}{2}$ and $\pm\frac{1}{2}$ separated by $(e^2qQ/2)(1+\eta^2/3)^{1/2}$. The resultant Mössbauer spectrum is a doublet with a separation called the quadrupole splitting of $\Delta = (e^2qQ/2)(1+\eta^2/3)^{1/2}$. When $\eta = 0$, $\Delta = e^2qQ/2$ or half the quadrupole coupling constant defined in nuclear quadrupole resonance spectroscopy. Typical energy level schemes for $\frac{1}{2} \rightarrow \frac{3}{2}$ and $\frac{7}{2} \rightarrow \frac{5}{2}$ (scaled to ^{129}I) transitions and the resultant spectra with relative line intensities for randomly oriented polycrystalline samples are illustrated in Fig.2.3.

The quadrupole spectrum is symmetrical only in the case of a $\frac{1}{2} \rightarrow \frac{3}{2}$ transition. In this particular instance there is no direct means of establishing the magnitude of η or the sign of V_{zz}. However, as detailed later in the chapter, it is possible to determine these parameters, either from the angular dependence of the line intensities in single crystals, or from the spectrum observed when a large external magnetic field is applied.

Once e^2qQ and η have been measured, they may be related to the chemical environment of the resonant nucleus. The coupling constant e^2qQ is the product of a nuclear constant (eQ) and the maximum value of V_{ij} (eq). Considerable confusion is often caused by referring to the sign of $V_{zz} = eq$ without specifying whether e is taken to be the charge of the electron or the proton. For this reason it is preferable to refer to the sign of e^2qQ or of q.

If $I_g = 0$ or $\frac{1}{2}$ so that $Q_g = 0$, then the magnitude of Q_e has to be established empirically by comparing the observed quadrupole splitting values with estimated values of V_{zz}. Fortunately, use of the quadrupole splitting is not entirely dependent on these intrinsically difficult calculations. The relative order of magnitude of e^2qQ can be related comparatively easily to the valence orbitals of the atom. The numerical value of V_{zz} due to an occupied electron orbital expressed by the wavefunction Ψ is given by the integral

$$\frac{V_{zz}}{e} = q = -\frac{(1-R)}{4\pi\epsilon_0}\int \Psi^*\left(\frac{3\cos^2\theta - 1}{r^3}\right)\Psi\, d\tau \qquad (2.19)$$

where $(1-R)$ is an empirical quantity less than unity, called the

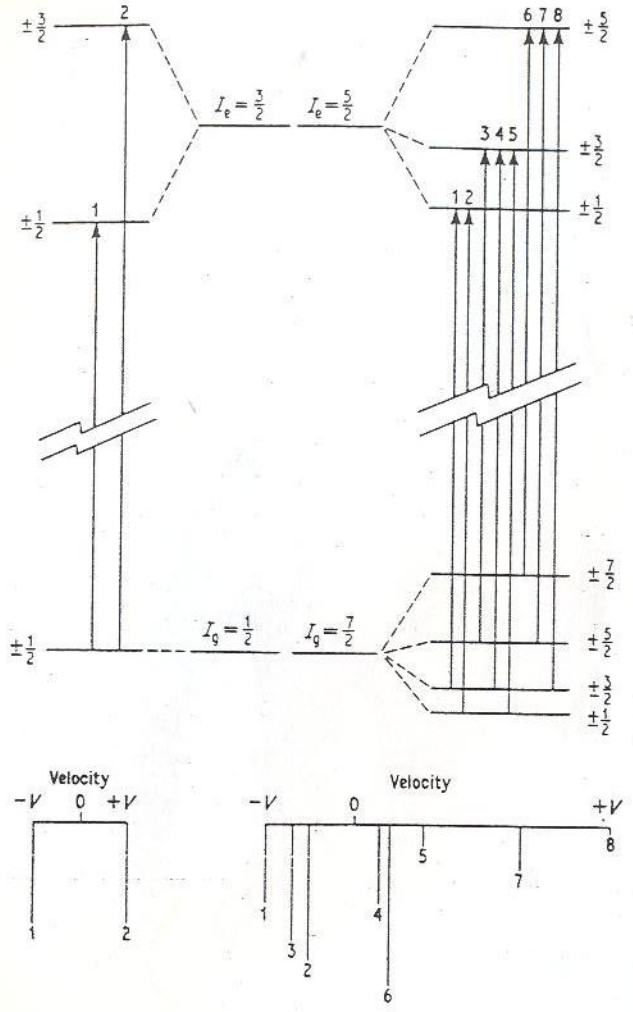

Fig. 2.3 The energy-level schemes and resultant spectra for quadrupole splitting of $I_g = \frac{1}{2} \rightarrow I_e = \frac{3}{2}$ and $I_g = \frac{7}{2} \rightarrow I_e = \frac{5}{2}$ (scaled to ^{129}I) transitions.

Sternheimer shielding factor, which allows for an opposing polarization of the inner core electrons [8]. Similarly

$$\eta = \frac{1}{q} \int \Psi^* \left(\frac{3 \sin^2 \theta \cos 2\phi}{r^3} \right) \Psi \, d\tau \qquad (2.20)$$

Table 2.1 The magnitude of q and η for the p- and d-orbitals

Orbital	$4\pi\epsilon_0 q/(1-R)$	η
p_z	$-\frac{4}{5}\langle r^{-3}\rangle$	0
p_x	$+\frac{2}{5}\langle r^{-3}\rangle$	−3
p_y	$+\frac{2}{5}\langle r^{-3}\rangle$	+3
$d_{x^2-y^2}$	$+\frac{4}{7}\langle r^{-3}\rangle$	0
d_{z^2}	$-\frac{4}{7}\langle r^{-3}\rangle$	0
d_{xy}	$+\frac{4}{7}\langle r^{-3}\rangle$	0
d_{xz}	$-\frac{2}{7}\langle r^{-3}\rangle$	+3
d_{yz}	$-\frac{2}{7}\langle r^{-3}\rangle$	−3

The magnitudes of q and η, expressed in units of the expectation value of $1/r^3$, are given in Table 2.1 for the conventional p- and d-orbitals.

The total value of q for a completely filled or half-filled shell of electrons is zero. An excess of electrons along the z axis (occupying p_z, d_{z^2}, d_{xz} or d_{yz}) results in a negative value of q, while an excess in the xy plane (p_x, p_y, d_{xy} or $d_{x^2-y^2}$) gives a positive value of q. The value of $\langle r^{-3}\rangle$ for a 4p-electron will be significantly smaller than that of a 3p-electron because of the greater radial extent of the former, and similarly a 3d-electron will give a smaller value than a 3p-electron, but probably greater than a 4p-electron. The spherically symmetric s-electron gives no electric field gradient. The sign and magnitude of e^2qQ can therefore be used empirically to measure the asymmetric occupation of the atomic valence orbitals, and many examples of this will be found in later chapters.

In some compounds the Mössbauer atom has an intrinsically high symmetry (e.g. the $Fe^{3+}d^5$ ion has a half-filled shell and is a spherical S-state ion) but may still show a quadrupole splitting. The latter originates from charges external to the atom, such as other ions, which polarize the spherical inner core and can induce a very large electric field gradient at the nucleus. This 'lattice' contribution summed over individual charges $Z_i e$ may be written as

$$\frac{V_{zz}}{e} = q_{\text{latt}} = \frac{(1-\gamma_\infty)}{4\pi\epsilon_0} \sum_i Z_i \frac{3\cos^2\theta - 1}{r_i^3} \qquad (2.21)$$

where γ_∞ is the Sternheimer antishielding factor [8]. This parameter expresses the core polarization and is usually large and negative. The lattice contribution also exists when the valence orbitals are asymmetrically occupied, but is usually acknowledged to be a minority contribution unless the co-ordinate geometry is very distorted. Formal attempts to subdivide q into valence and lattice terms are generally arbitrary and not altogether convincing.

2.4 Combined magnetic and quadrupole interactions

Both the magnetic and quadrupole hyperfine interactions express a directional interaction of the nucleus with its environment. However, when the two are present together, their respective principal axes are not necessarily co-linear, and it is not surprising therefore to find that the resultant behaviour can be much more complex. The formal Hamiltonian which is the sum of equations (2.9) and (2.12) has no general solution, but the predicted spectrum may always be obtained by numerical computation.

One of the few useful restricted solutions for a $\frac{1}{2} \rightarrow \frac{3}{2}$ transition is the case where the quadrupole interaction is very much weaker than the magnetic term, and can be treated as a small perturbation upon the latter. The resultant energy levels are given by

$$E_{QM} = -g\mu_N B m_z + (-1)^{|m_z|+1/2} \frac{e^2qQ}{4}\left(\frac{3\cos^2\theta - 1}{2}\right) \qquad (2.22)$$

where θ is the angle between the magnetic axis and the major axis of the electric field gradient tensor. All the magnetic hyperfine lines are shifted by a quantity

$$|\epsilon| = \frac{e^2qQ}{4}\left(\frac{3\cos^2\theta - 1}{2}\right) \qquad (2.23)$$

but the angle θ and the value of e^2qQ cannot be determined separately from the line positions. A schematic illustration of this is given in Fig.2.4. The presence of a small quadrupole perturbation is easily visible because the spectrum is no longer symmetrical about the centroid. If by chance $\cos\theta = 1/\sqrt{3}$ then the second term in equation (2.22) vanishes and the spectrum appears to be that

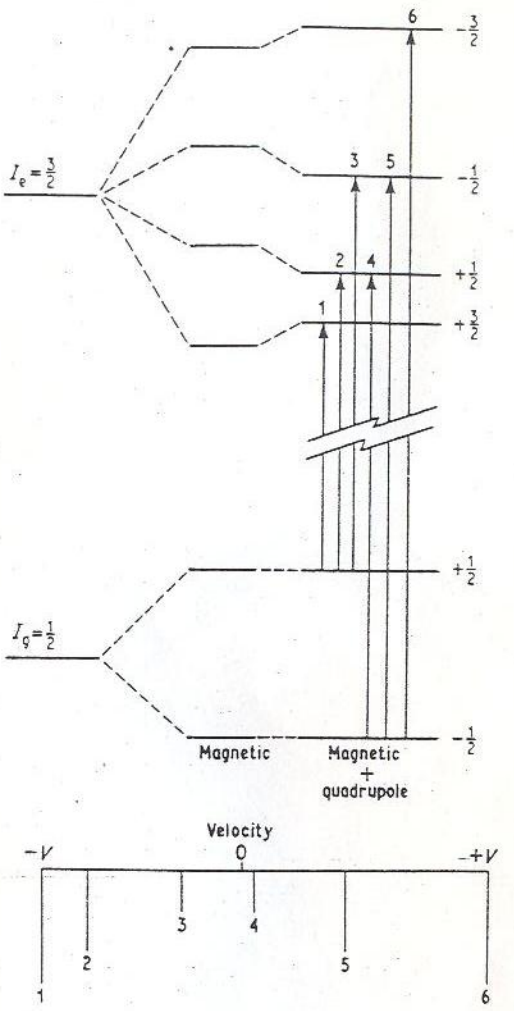

Fig. 2.4 The effect of a small quadrupole perturbation on a $\frac{1}{2} \rightarrow \frac{3}{2}$ magnetic hyperfine splitting. Lines 1 and 6 are shifted to more positive velocity by $+\epsilon$, while lines 2, 3, 4 and 5 are shifted by $-\epsilon$. The difference in the separations 1–2 and 5–6 is therefore 4ϵ.

of an unperturbed magnetic hyperfine splitting. Examples of combined magnetic/quadrupole interactions may be found on pp 115–116.

In the preceding section it was found that the sign of e^2qQ and the magnitude of η could not be determined from the quadrupole splitting of a $\frac{1}{2} \rightarrow \frac{3}{2}$ transition in a polycrystalline absorber because

the spectrum is symmetrical. One means of obtaining this information is to re-measure the spectrum in a large externally applied magnetic field with a magnetic flux density of 30–50 T. It is customary to apply the field parallel or perpendicular to the γ-ray beam. The resultant spectrum is of complex shape, reflecting the random orientation of the electric field gradient tensor with respect to the applied field, but is not symmetrical, so that the sign of e^2qQ is indicated. The shape of the spectrum may be calculated approximately by summing numerically the individual calculated spectra for a large number of orientations of the electric field gradient tensor.

One of the best examples of this method is given by the Fe^{57} resonance. The applied field splits the $\pm\frac{3}{2}$ component of the quadrupole spectrum into an apparent doublet, and the $\pm\frac{1}{2}$ component into an apparent triplet. Typical calculated spectrum envelopes are shown in Fig.2.5. The spectrum tends towards a symmetrical shape as η approaches unity (i.e. when $V_{zz} = -V_{yy}$ the sign of the major axis is indeterminate), and can be used to determine η to an accuracy of about ±0.05.

2.5 Relative line intensities

It was intimated in the preceding sections that the individual lines in a spectrum showing a hyperfine interaction have characteristic intensities which can be used to identify particular transitions. The magnitudes of the chemical isomer shift, the magnetic hyperfine field and the quadrupole splitting, can all be determined from the line positions alone, and the intensities merely used to confirm the assignment. If it is also desired to obtain the orientation of the magnetic axis or the electric field gradient tensor in an anisotropic sample such as a single crystal, then a more detailed knowledge of line intensities is essential.

The intensity of a particular hyperfine transition between quantized sub-levels is determined by the coupling of the two nuclear angular momentum states [9]. It can be expressed as the product of two terms which are angular-dependent and angular-independent respectively. Since the former averages to unity when all orientations are equally probable, e.g. in a randomly oriented polycrystalline powder sample, it is convenient to consider the angular-independent term first.

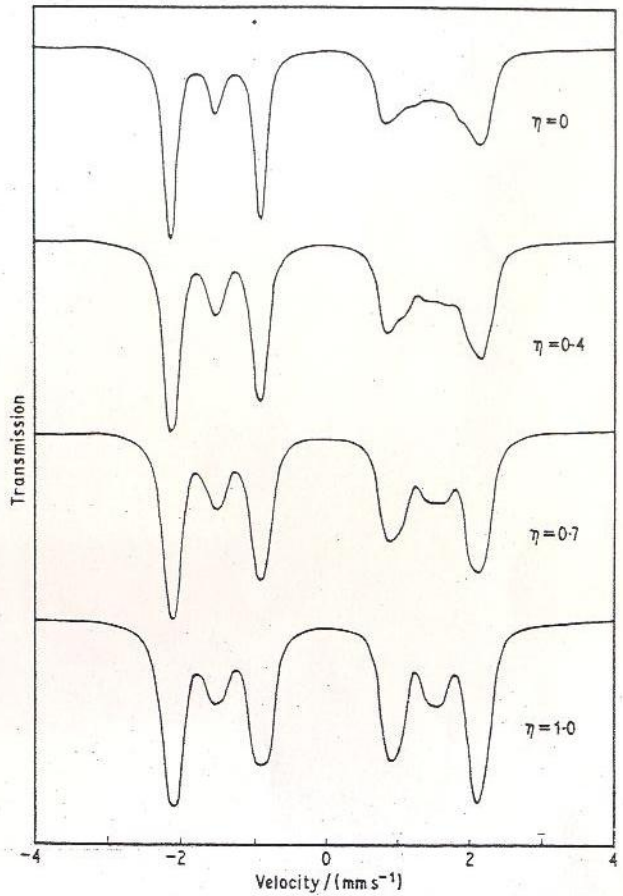

Fig. 2.5 Calculated spectra for a polycrystalline absorber giving an ^{57}Fe quadrupole splitting of $\Delta = 3$ mm s^{-1} and in an applied field with a flux density of 5 T parallel to the direction of observation. The spectrum becomes symmetrical as η tends towards unity. The sign of e^2qQ is positive in all cases.

The intensity in this instance is given by the square of the appropriate Clebsch-Gordan coefficient [10]

$$\text{Intensity } \alpha < I_1 J - m_1 m | I_2 m_2 >^2 \qquad (2.24)$$

where the two nuclear spin states I_1 and I_2 have I_z values of m_1 and m_2, and their coupling obeys the vector sums $J = I_1 + I_2$ and $m = m_1 - m_2$. J is referred to as the multipolarity of the transi-

tion, and the intensity is greater if J is small: if $J = 1$ it is referred to as a dipole transition, while with $J = 2$ it is a quadrupole transition. Most of the Mössbauer transitions take place without a change in parity, so that the radiation is classified as a magnetic dipole (M1) or electric quadrupole (E2) transition. One of the few exceptions is the 25.65-keV $\frac{5}{2}+ \rightarrow \frac{5}{2}-$ transition in ^{161}Dy which is an electric dipole (E1) transition. In some instances such as ^{99}Ru(90-keV) and ^{197}Au(77-keV) the radiation is a mixture of M1 and E2, and both terms must be added in the appropriate proportion. The selection rule for an M1 or E1 transition is $\Delta m_z = 0, \pm 1$, and for an E2 transition is $\Delta m_z = 0, \pm 1, \pm 2$.

The most frequently used coefficients are those for the $\frac{1}{2} \rightarrow \frac{3}{2}$ M1 transition, and these are given in Table 2.2 (coefficients for other spin states have been tabulated in [11]). I_1 may be either the ground or excited state spin. Although there are nominally eight transitions, the $+\frac{3}{2} \rightarrow -\frac{1}{2}$ and $-\frac{3}{2} \rightarrow +\frac{1}{2}$ transitions have a zero probability (forbidden). The six finite coefficients, C^2, which express the angular-independent intensity have a total probability of unit intensity and give directly the 3:2:1:1:2:3 intensity ratios for a magnetic hyperfine splitting, shown in Fig.2.2. The corresponding terms for a quadrupole spectrum are obtained by summation and give a 1:1 ratio.

The angular dependent terms, $\Theta(J, m)$, are expressed as the radiation probability in a direction at an angle θ to the quantization axis (i.e. the magnetic field axis or V_{zz}: note that the values in the table in the latter case are only correct if $\eta = 0$). The intensity for a polycrystalline sample is obtained by integration over all θ to obtain $\overline{\Theta(J, m)}$; e.g.

$$\tfrac{3}{2}\ \overline{\sin^2\theta} = \frac{1}{4\pi}\int_0^{2\pi}\int_0^{\pi}(\tfrac{3}{2}\sin^2\theta)\sin\theta\,d\theta\,d\phi = 1 \qquad (2.25)$$

and the total of emitted radiation is independent of θ and normalized to unity, i.e.

$$\sum_{m_1 m_2} \tfrac{1}{4}\langle I_1 J - m_1 m | I_2 m_2\rangle^2 \overline{\Theta(J, m)} = 1 \qquad (2.26)$$

Coefficients such as those in Table 2.2 are necessary to interpret

the angular dependence of the spectrum from a single crystal or oriented absorber. For example, a magnetically ordered metal alloy or oxide absorber may often be 'polarized' by magnetizing in a small external magnetic field to give a unique direction of the internal field. The expected line intensities can then be predicted from Table 2.2 to be in the ratios $3:x:1:1:x:3$ where $x = 4\sin^2\theta/(1 + \cos^2\theta)$; in particular the $m = 0$ transitions have a zero intensity when observed along the direction of the field ($\theta = 0°$) and a maximum intensity perpendicular to the field ($\theta = 90°$). This is illustrated schematically in Fig.2.6.

The equivalent behaviour in the quadrupole spectrum is a 1:3 ratio for the γ-ray axis parallel to the direction of V_{zz} and a 5:3 ratio perpendicular to V_{zz}. In this instance the angular dependence

Table 2.2 The relative probabilities for a $\frac{1}{2}, \frac{3}{2}$ transition

Magnetic spectra (M1)					
m_2	$-m_1$	m	C (1)	C^2 (2)	$\Theta(J, m)$ (2)
$+\frac{3}{2}$	$+\frac{1}{2}$	+1	1	$\frac{1}{4}$	$\frac{3}{4}(1 + \cos^2\theta)$
$+\frac{1}{2}$	$+\frac{1}{2}$	0	$\sqrt{\frac{2}{3}}$	$\frac{1}{6}$	$\frac{3}{2}\sin^2\theta$
$-\frac{1}{2}$	$+\frac{1}{2}$	−1	$\sqrt{\frac{1}{3}}$	$\frac{1}{12}$	$\frac{3}{4}(1 + \cos^2\theta)$
$-\frac{3}{2}$	$+\frac{1}{2}$	−2	0	0	–
$+\frac{3}{2}$	$-\frac{1}{2}$	+2	0	0	–
$+\frac{1}{2}$	$-\frac{1}{2}$	+1	$\sqrt{\frac{1}{3}}$	$\frac{1}{12}$	$\frac{3}{4}(1 + \cos^2\theta)$
$-\frac{1}{2}$	$-\frac{1}{2}$	0	$\sqrt{\frac{2}{3}}$	$\frac{1}{6}$	$\frac{3}{2}\sin^2\theta$
$-\frac{3}{2}$	$-\frac{1}{2}$	−1	1	$\frac{1}{4}$	$\frac{3}{4}(1 + \cos^2\theta)$

Quadrupole spectra (M1) when $\eta = 0$		
Transition	C^2 (2)	$\Theta(J, m)$ (2)
$\pm\frac{1}{2}, \pm\frac{1}{2}$	$\frac{1}{2}$	$\frac{1}{2} + \frac{3}{4}\sin^2\theta$
$\pm\frac{3}{2}, \pm\frac{1}{2}$	$\frac{1}{2}$	$\frac{3}{4}(1 + \cos^2\theta)$

(1) The Clebsch-Gordan coefficient $\langle\frac{1}{2}1 - m_1 m | \frac{3}{2}m_2\rangle$

(2) C^2 and $\Theta(J, m)$ are the angular-independent and angular-dependent terms normalized to a total radiation probability of

$$\sum_{m_1 m_2} C^2\Theta(J, m) = 1$$

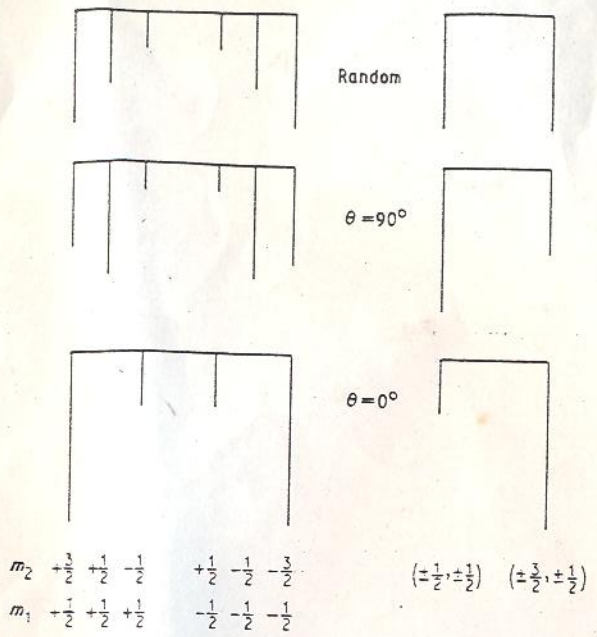

Fig. 2.6 The effect of orientation upon the relative line intensities of a magnetic hyperfine splitting and a quadrupole splitting of a $\frac{3}{2} \rightarrow \frac{1}{2}$ transition in an oriented absorber with a unique principal axis sytem.

can be used to determine which of the two lines is the $\pm\frac{1}{2} \rightarrow \pm\frac{3}{2}$ transition, and hence to obtain the sign of e^2qQ.

If there are combined magnetic and quadrupole interactions, or the asymmetry parameter η is non-zero, the previous discussion is no longer strictly valid. In these circumstances the energy states are no longer 'pure' states with a defined quantum number, and must be represented as linear combinations of terms. Likewise the intensity is obtained by an amplitude summation to allow for interference effects. These calculations are somewhat complex [11] and will not be described here.

The total cross-section for resonant absorption is a nuclear constant, so that the individual hyperfine lines are proportionately weaker than in an unsplit resonance line. This unfortunately necessitates a longer counting time to resolve the extra detail. In this discussion the absorption intensity has been considered for a single nucleus, but it is also important to consider the effects of finite absorber thickness (see p.11–12). The effective thickness of the

absorber $T_a = n_a \sigma_0 f_a$ is now multiplied by the fractional line intensity for each component $C^2\Theta(J, m)$, with the result that saturation of the absorption intensity occurs more quickly for the more intense resonance lines. This is seen as a dependence of the relative line intensities on increasing thickness which tends to decrease any asymmetry. In addition, the more intense lines have a larger linewidth due to the thickness broadening effect. Because of this, a quadrupole doublet spectrum of for example a single crystal with the direction of observation parallel to V_{zz} will show a line intensity ratio much less than 1:3.

An additional complication which also affects the intensities appreciably is polarization of the incident γ-ray beam as it progresses through the crystal [12]. For these reasons, unless it is proposed to attempt a somewhat difficult thickness correction, it is necessary to obtain relative intensity data from very thin absorbers. However, the possibility of underestimation of any asymmetry should always be borne in mind.

There are two other important influences on relative line intensities which are of particular importance in powders. If the compacted polycrystalline powder has a tendency towards partial orientation (texture), then the values of $\Theta(J, m)$ do not average to unity, and there is some residual asymmetry in the spectrum which is angular dependent. This effect can be quite large, and exceedingly difficult to eliminate in fibrous or platelike materials. A second effect which is similar in many ways is the Goldanskii-Karyagin effect, in which anisotropy of the recoilless fraction results in an asymmetry which is not angular dependent but is usually small. This is discussed in more detail in Chapter 6. In many instances deviations from the 1:1 line intensity ratio in a $\frac{1}{2} \rightarrow \frac{3}{2}$ quadrupole doublet have been attributed to the Goldanskii-Karyagin effect without convincing proof that there was no residual texture in the sample.

References

[1] Pound, R. V. and Rebka, G. A. (1959) *Phys. Rev. Letters*, 3, 554.
[2] Kistner, O. C. and Sunyar, A. W. (1960) *Phys. Rev. Letters*, 4, 412.
[3] Breit, G. (1958) *Rev. Mod. Phys.*, 30, 507.
[4] Reddy, K. R., Barros, F. de S. and DeBenedetti, S. (1966) *Phys. Letters*, 20, 297.
[5] Pound, R. V. and Rebka, G. A. (1960) *Phys. Rev. Letters*, 4, 274.